Palestine Journal of Mathematics

Vol. 11(Special Issue I)(2022) , 95–108

HALL EFFECT ON UNSTEADY MHD 3D CARREAU NANOFLUID FLOW PAST A STRETCHING SHEET WITH NAVIER'S SLIP AND NONLINEAR THERMAL RADIATION

Manik Das, Susmay Nandi and Bidyasagar Kumbhakar

Communicated by Muslim Malik

MSC 2010 Classifications: 76A05, 76W05, 80A19, 80A21, 80A32.

Keywords and phrases: Magnetohydrodynamics (MHD), Thermal radiation, Heat generation, Activation energy, Navier's slip, Hall effect.

Abstract This study examines the unsteady and incompressible MHD Carreau nanofluid flow induced by a stretching sheet considering Hall effect, nonlinear thermal radiation, velocity slips, heat generation, chemical reaction, and activation energy. It is also assumed that a zero mass flow condition exists at the surface. To approximate heat flux due to radiation, Rosseland's estimation has been used. The controlling PDEs are metamorphosed into a system of ODEs using appropriate similarity transformations. The resultant nonlinear equations are numerically solved in MATLAB using the *bvp4c* solver. The many physical variables that influence velocity, temperature, and concentration distributions are illustrated through diagrams. For various key parameters, the fluctuations in shear stresses, heat and mass transport rates at the sheet are discussed and displayed in the form of table. The results obtained for a specific case of the current problem are then compared with the findings that have already been published, and the comparison reveals a good agreement among the results. Graphical results show that Navier's slip has the tendency to diminish the fluid velocity. The temperature of the fluid is enhanced for thermal radiation and heat generation.

1 Introduction

Theoretical/experimental study of non-Newtonian fluid flows has been a significant topic of research in recent years due to its importance in a variety of industrial and engineering phenomena. It's worth noting that in the case of non-Newtonian fluids, the stress-strain relationship is nonlinear. Due to the highly non-linearity of the model equations, researchers faced numerous hurdles in analyzing such fluid flow problems. In heat transfer procedures using non-Newtonian fluids, shear impacts are important. Paints, liquid detergents, multi-grade oil, blood delivered in a microcirculatory system, printer ink, muck, sauce and other non-Newtonian fluids are only a few examples. Cortell [5] investigated the flow of an electrically conducting second-grade nanofluid passed through a semi-infinite porous stretching sheet subjected to a uniform transverse magnetic field. AbdEl-Gaied and Hamad [1] demonstrated the mixed convective alumina-water nanofluid flow along with a moving permeable vertical flat plate under the influence of a magnetic field applied normal to the plate. MHD viscoelastic fluid flow through an extending vertical surface in a porous media was studied by Turkyilmazoglu [36]. Eid and Mahny [8] explored the cumulative influence of a magnetic field and heat source/sink on unsteady non-Newtonian nanofluid flow over a permeable stretched wall. Tian et al. [35] looked into the mixed convection in unsteady 2D viscous and electrically conducting nanofluid flow past a stretching plate with convective thermal boundary conditions.

Due to overwhelming applications of thermal radiation in aircraft, gas turbines, satellites, missiles, and space vehicles ([18], [3]), many researchers have explored the effects of thermal radiation on MHD flows. However, in most cases, a linear variation in thermal radiation has been considered. But, it is worth mentioning that, in several heat transfer processes involving high temperature, a linear model for thermal radiation doesn't provide appropriate results. In such a case, a nonlinear variation in thermal radiation may lead to a better result. So, in view

Nomenclature

S	Unsteadiness parameter	Sh_x	Local Sherwood number
x, y, z	Space coordinate	N	Buoyancy ratio parameter
n	Power-law-index	Nb	Brownian motion parameter
T_∞	Ambient temperature	g	Magnitude of gravitational acceleration
C_∞	concentration	D_T	Coefficient of thermal diffusion
u, v, w	Velocity components	Bi	Biot number
n^*	Fitted rate constant		
K_r^2	Chemical reaction coefficient	**Greek**	**Symbols**
u_w,v_w	Stretching velocities	β	Dimensional unsteadiness parameter
k	Thermal conductivity	ν	Kinetic viscosity
Q_1	Heat generation coefficient	β_C, β_C^*	Linear and nonlinear coefficients
D_B	Mass diffusivity		of concentration expansion
Pr	Prandtl number	μ	Dynamic viscosity
E	Dimensionless activation energy	Γ_1	Chemical reaction parameters
c_p	Specific heat	σ	Electrical conductivity
Nt	Thermophoresis parameter	κ	Boltzmann constant
Le	Lewis number	ζ_T, ζ_C	Non linear convection parameter
N_1, N_2	Velocity slip coefficients	σ^*	Stefan-Boltzmann constant
We_1, We_2	Weissenberg numbers	θ	Dimensionless temperature
B_0	Constant magnetic field	δ	Heat generation parameter
E_a	Activation energy	α	Thermal diffusivity
M	Magnetic parameter	ϕ	Dimensionless concentration
k^*	Mean absorption coefficient	α_1, α_2	Velocity slip parameters
Rd	Thermal radiation parameter	ρ	Density
T, C	Temperature and concentration	θ_w	Temperature ratio parameter
C_{fx}, C_{fy}	Local skin friction coefficients	β_1	Velocity ratio parameter
m	Hall parameter	τ	Ratio between effective heat capacity
Nu_x	Local Nusselt number		of nanoparticles and base fluid
T_w	Surface temperature	β_T, β_T^*	Linear and non-linear Thermal
C_w	Surface concentration		expansion coefficients
L	Dimensionless quantity	λ	Mixed convection parameter

of such facts, Hayat and Qasim [12] illustrated the role of thermal radiation on MHD Maxwell fluid flow across a stretching sheet with mixed convection and thermophoresis. Rashidi et al. [25] studied MHD convective water-based nanofluid flow past a vertically extended sheet while taking heat radiation into account. Using Buongiorno's model, Daniel et al. [6] conducted a study to examine the effects of thermal radiation, viscous-Joule dissipations on MHD nanofluid flow through a porous stretchable sheet. Shah et al. [28] conducted thermal radiation experiments on the MHD CNTs nanofluid flow passing through a stretched sheet with rotation. Gireesha et al. [10] surveyed the effects of nonlinear thermal radiation on the flow of MHD 3D Jeffrey nanofluid across a nonlinearly permeable stretched sheet, considering various aspects of the problem.

Swiss scientist Svante Arrhenius first coined the phrase "activation energy" in the year 1889. He clarified that activation energy is the energy recovered during a chemical reaction control. It also shows how little energy is required to start a chemical reaction process. The activation energy theory is useful in various fields, including oil reservoirs, chemical engineering, food processing, and geothermal engineering. Based on the mentioned applications, in the presence of a chemical reaction, the effect of mass transfer in the magnetohydrodynamic flow of a Casson fluid past a porous stretching sheet is described by Shehzad et al. [31]. Mustafa et al. [21] explored the hydromagnetic nanofluid flow over a vertical surface, taking into account the impact of activation energy and buoyancy force. Goqo et al. [11] discussed MHD viscous nanofluid flow along with a porous wedge in the presence of chemical reactions. They accounted for both heat radiation and mixed convection while doing so. The inspection on activation energy in

3D unsteady Carreau nanofluid flow past a stretching sheet due to heat source/sink and mixed convection was carried out by Irfan et al. [15]. On account of nonlinear mixed convection, Brownian motion, and thermophoretic diffusion, Irfan [16] studied the effect of chemical reaction on unsteady Carreau nanofluid flow near a stretching sheet.

If the applied magnetic field intensity is very strong or the fluid density is very low, Hall current becomes considerable (like ionized fluid). In such instances, the electric current is usually carried by electrons that collide with other neutral or charged particles on a regular basis. When an electric field is sufficiently strong, the conductivity parallel to it drops, causing a current to flow in the direction perpendicular to both magnetic and electric fields. Hall effect is the name given to this occurrence, while Hall current is the name given to the current. The Hall effect finds noteworthy applications in nuclear power reactors, Hall current accelerators, magnetometers, energy storage systems, etc. ([33], [34]). Depending on the applications, Shit and Haldar [32] looked at the cumulative influence of Hall current and thermal radiation on hydromagnetic free-convective flow along an inclined stretchable surface with varying viscosity and heat generation/absorption. Prasad et al. [24] studied the influence of the Hall effect on MHD electrically conducting fluid flow over a stretching surface of varied thickness. Khan et al. [17] investigated the Hall effect in MHD thin-film second-grade nanofluid flow with Brownian motion, thermophoresis, and heat transfer through a stretched sheet. Nandi and Kumbhakar [23] investigated the Hall effect on MHD natural convection flow of an optically thick radiating fluid along with an oscillating vertical plate with chemical reactions and heat generation/absorption.

For a boundary layer flow, the no-slip condition at the surface is a commonly used boundary condition. In 1823, Navier discovered that the velocity slip at the solid wall varied linearly with the shear stress. It has a various of applications in lubricants, artificial heart valves, biological fluids, internal cavities, and medical sciences, etc ([26], [20], [27],[30], [7]). Keeping in mind the concept of no-slip condition, Hayat et al. [13] examined the effects of nonlinear thermal radiation and velocity slip effects on MHD 3D nanoliquid flow past a stretching sheet. In order to understand how MHD Casson nanofluid flow is affected by velocity slip, chemical reaction, and convective boundary conditions, Ibrahim et al. [14] analyzed these different aspects for MHD Casson nanofluid flow along with a nonlinearly stretching sheet. Aziz and Jamshed [2] illustrated unsteady MHD boundary layer slip flow of a power-law fluid near a porous nonlinearly stretching sheet. Nandi and Kumbhakar [22] investigated unsteady MHD fluid flow along with a permeable infinite flat plate with surface slippage while accounting for Hall current, thermal radiation, and internal heat generation/absorption.

Motivated by the literature mentioned above, the primary goal of this study is to analyze 3-dimensional, unsteady and incompressible MHD Carreau nanofluid flow over a stretching surface with Hall effect, velocity slips and nonlinear thermal radiation. Internal heat generation, chemical reaction, activation energy, convecting heating, and zero mass flux are also taken into account. Well-matched conversions produce nonlinear ODEs, and *bvp4c* in-built MATLAB routine is utilized to solve those equations. Parameters that show significant impacts on the flow, thermal and concentration fields are discussed with the help of graphs. For a limiting case, the obtained results are compared with the results reported in existing studies, and good agreement is observed.

2 Mathematical model equations

Consider a 3-dimensional, unsteady and incompressible MHD Carreau nanofluid flow along a stretching surface with velocity slip, Hall effects. Nonlinear thermal radiation, heat generation, and chemical reaction with activation energy are all included in the analysis. The sheet is positioned in the rectangular coordinate frame (x, y, z) where the x-axis is directed along the sheet surface towards the flow direction. The y-axis is directed along the width, and the z-axis is perpendicular to the surface. A time-dependent magnetic field of magnitude $B(t)$ is applied along the z-direction. The surface is stretched along x and y-directions with velocities $u_{\mathrm{w}} = \frac{ax}{1-\beta t}$ and $v_{\mathrm{w}} = \frac{by}{1-\beta t}$ (a, b being positive constants) respectively. The nanofluid temperature and species concentration at the surface are kept at constant values of T_{w} and C_{w} respectively, whereas the ambient fluid temperature and species concentration are maintained at constant values of T_∞ and C_∞ respectively.

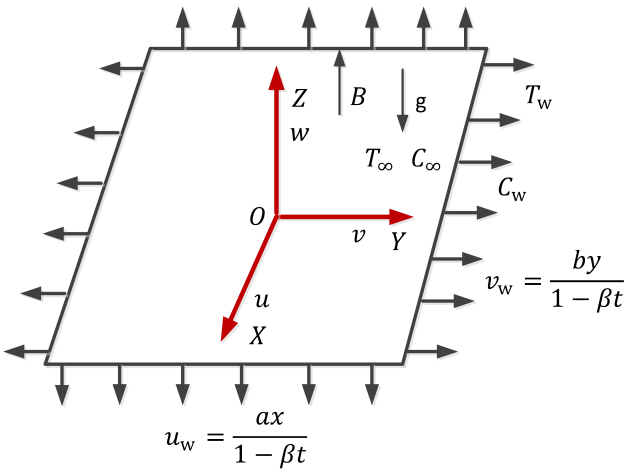

Figure 1. Geometry describing the flow problem

The following fluid flow equations for the current problem may be modelled with the assumptions stated above: ([15], [16]):

$$\frac{\partial u}{\partial x}+\frac{\partial v}{\partial y}+\frac{\partial w}{\partial z}=0, \tag{2.1}$$

$$\begin{aligned}\frac{\partial u}{\partial t}+u\frac{\partial u}{\partial x}+v\frac{\partial u}{\partial y}+w\frac{\partial u}{\partial z}&=\frac{\sigma B^2(t)}{\rho_f(1+m^2)}(mv-u)\\&+\mathrm{g}\left[\beta_T(T-T_\infty)+\beta_T^*(T-T_\infty)^2+\beta_C(C-C_\infty)+\beta_C^*(C-C_\infty)^2\right]\\&+\nu\left(\frac{\partial^2 u}{\partial z^2}\right)\left[\left\{1+\left(\Gamma\frac{\partial u}{\partial z}\right)^2\right\}^{\frac{n-1}{2}}+(n-1)\left(\Gamma\frac{\partial u}{\partial z}\right)^2\left\{1+\left(\Gamma\frac{\partial u}{\partial z}\right)^2\right\}^{\frac{n-3}{2}}\right],\end{aligned} \tag{2.2}$$

$$\begin{aligned}\frac{\partial v}{\partial t}+u\frac{\partial v}{\partial x}+v\frac{\partial v}{\partial y}+w\frac{\partial v}{\partial z}&=-\frac{\sigma B^2(t)}{\rho_f(1+m^2)}(mu+v)\\&+\nu\left(\frac{\partial^2 v}{\partial z^2}\right)\left[\left\{1+\left(\Gamma\frac{\partial v}{\partial z}\right)^2\right\}^{\frac{n-1}{2}}+(n-1)\left(\Gamma\frac{\partial v}{\partial z}\right)^2\left\{1+\left(\Gamma\frac{\partial v}{\partial z}\right)^2\right\}^{\frac{n-3}{2}}\right],\end{aligned} \tag{2.3}$$

$$\begin{aligned}\frac{\partial T}{\partial t}+u\frac{\partial T}{\partial x}+v\frac{\partial T}{\partial y}+w\frac{\partial T}{\partial z}=&\alpha\frac{\partial^2 T}{\partial z^2}+\tau\left\{D_B\frac{\partial T}{\partial z}\frac{\partial C}{\partial z}+\frac{D_T}{T_\infty}\left(\frac{\partial T}{\partial z}\right)^2\right\}\\&-\frac{1}{(\rho c_p)_f}\frac{\partial q_r}{\partial z}+\frac{Q_1}{(\rho c_p)_f}(T-T_\infty),\end{aligned} \tag{2.4}$$

$$\frac{\partial C}{\partial t}+u\frac{\partial C}{\partial x}+v\frac{\partial C}{\partial y}+w\frac{\partial C}{\partial z}=D_B\frac{\partial^2 C}{\partial z^2}+\frac{D_T}{T_\infty}\frac{\partial^2 T}{\partial z^2}-k_r^2(C-C_\infty)\left(\frac{T}{T_\infty}\right)^{n^*}e^{\left(\frac{-E_a}{\kappa T}\right)}. \tag{2.5}$$

The physical boundary conditions for the current problem are given as follows:

$$\left.\begin{aligned}&u=u_w+N_1\nu_f\frac{\partial u}{\partial z},\ v=v_w+N_2\nu_f\frac{\partial v}{\partial z},\ w=0,\ -k\frac{\partial T}{\partial z}=h_f(T_w-T),\\&D_B\frac{\partial C}{\partial z}+\frac{D_T}{T_\infty}\frac{\partial T}{\partial z}=0,\ \text{at } z=0,\\&u\to 0,\quad v\to 0,\quad T\to T_\infty,\quad C\to C_\infty\quad \text{as}\quad z\to\infty.\end{aligned}\right\} \tag{2.6}$$

While simulating the present radiative heat transfer problem, the following Rosseland's approximation is assumed ([9]):

$$q_r = -\frac{16\sigma^* T^3}{3k^*}\frac{\partial T}{\partial z}. \tag{2.7}$$

The energy equation takes the form after applying expression (2.7) to equation (2.4)

$$\begin{aligned}\frac{\partial T}{\partial t} + u\frac{\partial T}{\partial x} + v\frac{\partial T}{\partial y} + w\frac{\partial T}{\partial z} =& \alpha\frac{\partial^2 T}{\partial z^2} + \tau\left\{D_B\frac{\partial T}{\partial z}\frac{\partial C}{\partial z} + \frac{D_T}{T_\infty}\left(\frac{\partial T}{\partial z}\right)^2\right\} \\ &+ \frac{16\sigma^* T^2}{3\left(\rho c_p\right)_f k^*}\left\{T\frac{\partial^2 T}{\partial Z^2} + 3\left(\frac{\partial T}{\partial Z}\right)^2\right\} \\ &+ \frac{Q_1}{\left(\rho c_p\right)_f}\left(T - T_\infty\right).\end{aligned} \tag{2.8}$$

The variable aspects of wall temperature, wall concentration and time-dependent magnetic field are considered as ([16]):

$$T_{\mathrm{w}}(x,t) = \frac{T_0 x u_{\mathrm{w}}}{\nu(1-\beta t)^{\frac{1}{2}}} + T_\infty, \quad C_{\mathrm{w}}(x,t) = \frac{C_0 x u_{\mathrm{w}}}{\nu(1-\beta t)^{\frac{1}{2}}} + C_\infty, \quad B(t) = \frac{B_0}{(1-\beta t)^{\frac{1}{2}}}.$$

To obtain similar solutions of equations (2.2), (2.3), (2.8) and (2.5) subject to the boundary conditions (2.6), the following similarity transformations are introduced:

$$\left.\begin{aligned} &u = \frac{ax}{1-\beta t}f'(\eta), \quad v = \frac{ay}{1-\beta t}g'(\eta), \quad w = -\sqrt{\frac{a\nu}{1-\beta t}}\left\{f(\eta) + g(\eta)\right\}, \\ &\theta(\eta) = \frac{T - T_\infty}{T_{\mathrm{w}} - T_\infty}, \quad \phi(\eta) = \frac{C - C_\infty}{C_{\mathrm{w}} - C_\infty}, \quad \eta = z\sqrt{\frac{a}{\nu(1-\beta t)}}. \end{aligned}\right\} \tag{2.9}$$

Substitution of the above transformations in equations (2.2), (2.3), (2.8) and (2.5) yields the following ordinary differential equations:

$$\begin{aligned} f'''\left[1 + nWe_1^2 f''^2\right]\left[1 + We_1^2 f''^2\right]^{\frac{n-3}{2}} - f'^2 + \left(f + g\right)f'' - S\left(f' + \frac{1}{2}\eta f''\right) \\ + \frac{M}{1+m^2}\left(mLg' - f'\right) + \lambda\left(1 + \zeta_T\theta\right)\theta + \lambda N\left(1 + \zeta_C\phi\right)\phi = 0, \end{aligned} \tag{2.10}$$

$$\begin{aligned} g'''\left[1 + nWe_2^2 g''^2\right]\left[1 + We_2^2 g''^2\right]^{\frac{n-3}{2}} - g'^2 + \left(f + g\right)g'' - S\left(g' + \frac{1}{2}\eta g''\right) \\ - \frac{M}{1+m^2}\left(m\frac{1}{L}f' + g'\right) = 0, \end{aligned} \tag{2.11}$$

$$\begin{aligned} \theta'' + Pr\left(f + g\right)\theta' - Pr\frac{S}{2}(3\theta + \eta\theta') - 2Pr\theta f' + PrNb\theta'\phi' + PrNt\theta'^2 + Pr\delta\theta \\ + Rd\left\{1 + \theta\left(\theta_{\mathrm{w}} - 1\right)\right\}^2\left[3\theta'^2\left(\theta_{\mathrm{w}} - 1\right) + \left\{1 + \theta\left(\theta_{\mathrm{w}} - 1\right)\right\}\theta''\right] = 0, \end{aligned} \tag{2.12}$$

$$\begin{aligned} \phi'' + PrLe\left(f + g\right)\phi' - PrLe\frac{S}{2}(3\phi + \eta\phi') - 2PrLe\phi f' + \frac{Nt}{Nb}\theta'' \\ - PrLe\Gamma_1\left\{1 + (\theta_{\mathrm{w}} - 1)\theta\right\}^{n^*} e^{-\frac{E}{1+(\theta_{\mathrm{w}}-1)\theta}}\phi = 0. \end{aligned} \tag{2.13}$$

Boundary conditions, in dimensionless form, are stated as

$$\left.\begin{aligned} &f(0) = 0, \quad f'(0) = 1 + \alpha_1 f''(0), \quad g(0) = 0, \quad g'(0) = \beta_1 + \alpha_2 g''(0), \\ &\theta'(0) = -Bi\left\{1 - \theta(0)\right\}, \quad \phi'(0) = -\frac{Nt}{Nb}\theta'(0), \\ &f'(\infty) \to 0, \quad g'(\infty) \to 0, \quad \theta(\infty) \to 0, \quad \phi(\infty) \to 0, \end{aligned}\right\} \tag{2.14}$$

where

$$We_1 = \sqrt{\frac{\Gamma^2 a u_{\mathrm{w}}^2}{\nu(1-\beta t)}}, \quad We_2 = \sqrt{\frac{\Gamma^2 a v_{\mathrm{w}}^2}{\beta_1^2 \nu(1-\beta t)}}, \quad N = \frac{\beta_C (C_{\mathrm{w}} - C_\infty)}{\beta_T (T_{\mathrm{w}} - T_\infty)}, \quad M = \frac{\sigma B_0^2}{a\rho_f},$$
$$\lambda = \frac{\mathrm{g}\beta_T (1-\beta t)(T_{\mathrm{w}} - T_\infty)}{a u_{\mathrm{w}}}, \quad \alpha = \frac{k}{(\rho c_p)_f}, \quad Pr = \frac{\nu}{\alpha}, \quad Nb = \frac{\tau D_B (C_{\mathrm{w}} - C_\infty)}{\nu},$$
$$Nt = \frac{\tau D_T (T_{\mathrm{w}} - T_\infty)}{\nu T_\infty}, \quad Le = \frac{\alpha}{D_B}, \quad \Gamma_1 = \frac{k_r^2 (1-\beta t)}{a}, \quad \theta_{\mathrm{w}} = \frac{T_{\mathrm{w}}}{T_\infty}, \quad E = \frac{E_a}{\kappa T_\infty},$$
$$\alpha_1 = N_1 \nu_f \sqrt{\frac{a}{\nu(1-\beta t)}}, \quad \alpha_2 = N_2 \nu_f \sqrt{\frac{a}{\nu(1-\beta t)}} \quad \beta_1 = \frac{b}{a}, \; Bi = \frac{h_f}{k}\sqrt{\frac{\nu(1-\beta t)}{a}},$$
$$\zeta_T = \frac{\beta_T^* (T_{\mathrm{w}} - T_\infty)}{\beta_T}, \quad \zeta_C = \frac{\beta_C^* (C_{\mathrm{w}} - C_\infty)}{\beta_C}, \quad \delta = \frac{Q_1(1-\beta t)}{a(\rho c_p)_f}, \quad Rd = \frac{16\sigma^* T_\infty^3}{3(\rho c_p)_f \alpha k^*},$$
$$L = \frac{y}{x}, \quad S = \frac{\beta}{a}.$$

3 Physical quantities of engineering interest

When addressing the problem from an engineering perspective, the only physical quantities of importance are the coefficients local skin-friction, Nusselt and Sherwood numbers which are expressed as

$$C_{fx} = \frac{2\nu}{u_{\mathrm{w}}^2}\left[\frac{\partial u}{\partial z}\left\{1 + \left(\Gamma \frac{\partial u}{\partial z}\right)^2\right\}^{\frac{n-1}{2}}\right]_{z=0}, \tag{3.1}$$

$$C_{fy} = \frac{2\nu}{v_{\mathrm{w}}^2}\left[\frac{\partial v}{\partial z}\left\{1 + \left(\Gamma \frac{\partial v}{\partial z}\right)^2\right\}^{\frac{n-1}{2}}\right]_{z=0}, \tag{3.2}$$

$$Nu_x = -\frac{x}{k\,(T_{\mathrm{w}} - T_\infty)}\left[\left(k + \frac{16\sigma^* T^3}{3k^*}\right)\frac{\partial T}{\partial z}\right]_{z=0}, \tag{3.3}$$

$$Sh_x = -\frac{x D_B}{D_B\,(C_{\mathrm{w}} - C_\infty)}\left(\frac{\partial C}{\partial z}\right)_{z=0}. \tag{3.4}$$

The aforementioned physical quantities can be expressed, in non-dimensional form, using the dimensionless variables specified in (2.9)

$$C_{fx}\sqrt{Re_x} = 2f''(0)\left[1 + We_1^2 f''^2(0)\right]^{\frac{n-1}{2}}, \tag{3.5}$$

$$C_{fy}\sqrt{Re_y} = 2(\beta_1)^{\frac{-3}{2}} g''(0)\left[1 + We_2^2 g''^2(0)\right]^{\frac{n-1}{2}}, \tag{3.6}$$

$$\frac{Nu_x}{\sqrt{Re_x}} = -\left[1 + Rd\left\{1 + (\theta_{\mathrm{w}} - 1)\,\theta(0)\right\}^3\right]\theta'(0), \tag{3.7}$$

$$\frac{Sh_x}{\sqrt{Re_x}} = -\phi'(0), \tag{3.8}$$

where $(Re_x, Re_y) = \left(\frac{u_{\mathrm{w}} x}{\nu}, \frac{v_{\mathrm{w}} y}{\nu}\right)$ denote the local Reynolds numbers.

4 Implementation of numerical technique

4.1 Solution procedure

Numerical solutions are obtained for the highly nonlinear ODEs (2.10)-(2.13) subject to the constraints defined in (2.14) by employing *bvp4c* in-built solver in MATLAB. The basic method of solution using *bvp4c* is based on four points Lobatto collocation formula. It uses polynomial type collocation, and its order is four. The higher-order equations (2.10)-(2.13) are converted into a set of first-order equations. Furthermore, while implementing the solution technique, the boundary value problem is metamorphosed into an initial value problem by assuming suitable guess values to those missing initial conditions. To achieve the far-field conditions, a finite fixed value of η, say $\eta = 10$, has been considered. With this assumption, all the conditions specified outside the boundary layer are satisfied.

Table 1. Comparative results of $-f''(0)$ for altered values of S

	$-f''(0)$			
S	Ref. [29]	Ref. [4]	Ref. [16]	Present result
0.8	1.261042	1.261512	1.261044	1.261043
1.2	1.377722	1.378052	1.377728	1.377725
2.0	1.587362	–	1.587381	1.587370

Table 2. Comparative results of $-f''(0)$ and $-g''(0)$ for altered values of β_1

	$-f''(0)$			$-g''(0)$		
β_1	Ref. [37]	Ref. [19]	Present results	Ref. [37]	Ref. [19]	Present results
0	1	1	1.000008	0	0	0
0.25	1.048813	1.048813	1.048813	0.194564	0.194565	0.194565
0.50	1.093097	1.093096	1.093096	0.465205	0.465206	0.465206
0.75	1.134485	1.134486	1.134486	0.794622	0.794619	0.794619
1	1.173720	1.173721	1.173721	1.173720	1.173721	1.173721

4.2 Results validation

The numerical values of $-f''(0)$ displayed in Table 1 have been computed for different values of unsteadiness parameter S for a specific case of the current problem, i.e., when $We_1 = We_2 = \lambda = \zeta_T = \zeta_C = M = \alpha_1 = \alpha_2 = \beta_1 = N = 0$ and $n = 1$. In order to check the correctness of the results and the reliability of the employed numerical approach, these values are compared with the results reported by Sharidan et al. [29], Chamkha et al. [4] and Irfan [16]. Further, another comparison of values of $-f''(0)$ and $-g''(0)$ w.r.t. β_1 when $We_1 = We_2 = \lambda = \zeta_T = \zeta_C = M = \alpha_1 = \alpha_2 = N = S = 0$ and $n = 1$ is presented in Table 2. These results are compared with those of Wang [37] and Liu and Anderson [19]. Both the tables clearly reveal that there exists a nice agreement among the results.

5 Results and Discussion

In this part, the effects of several relevant flow factors such as M, S, m, α_1, α_2, Rd, δ, Bi, Nb, Nt, Γ_1 and E on the flow-field, temperature, and concentration scatterings are examined and demonstrated using Figures 2-19. The behavior of suface shear stresses, heat and mass transfer rates at the wall is demonstrated by computing their numerical values, which are shown in Tables 3 and 4. To carry out numerical implementation, the default values of relevant parameters are assumed as $We_1 = We_2 = 1.6$, $\lambda_1 = N = n = m = L = E = 0.5$, $Pr = 1.4$, $Nt = Nb = \zeta_T = \zeta_C = 0.4$, $Rd = \delta = \alpha_1 = \alpha_2 = 0.3$, $S = Le = 1.5$, $M = 2$, $\beta_1 = 0.6$,

$Bi = n^* = 0.2$, $\Gamma_1 = 0.6$ and $\theta_w = 1.1$ by consulting some good research articles relevant to the present work. These values are maintained unaltered throughout the investigation except the changing parameter as specified in the corresponding tables and figures .

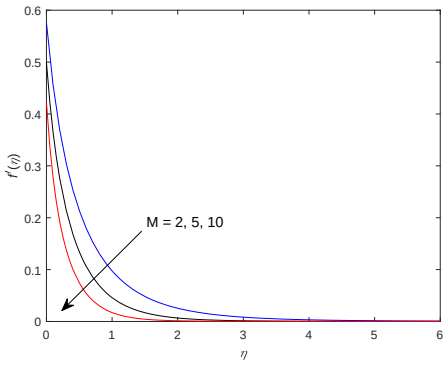

Figure 2. Depiction of $f'(\eta)$ vs M

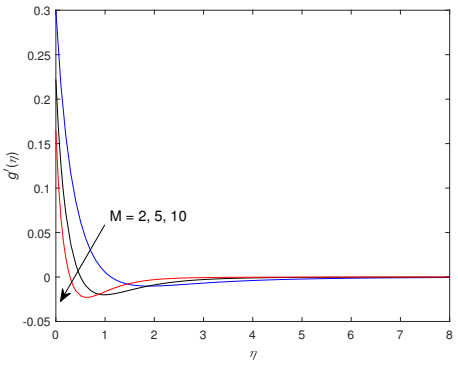

Figure 3. Depiction of $g'(\eta)$ vs M

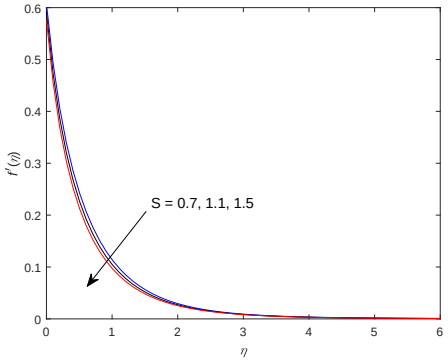

Figure 4. Depiction of $f'(\eta)$ vs S

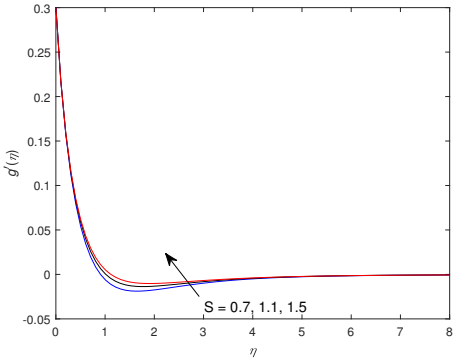

Figure 5. Depiction of $g'(\eta)$ vs S

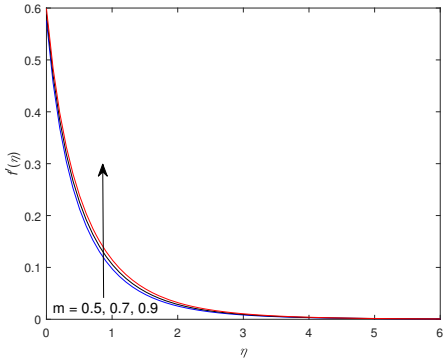

Figure 6. Depiction of $f'(\eta)$ vs m

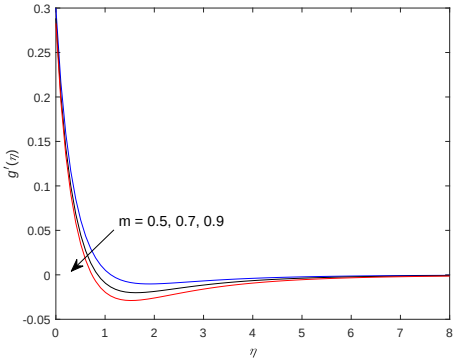

Figure 7. Depiction of $g'(\eta)$ vs m

The effects of M, S, m, α_1 and α_2 on the velocity field are depicted in Figures 2-9. In both the directions, the flow is decelerated for increasing values of M which is shown in Figures 2 and 3. This is due to the reason that higher magnetic parameter creates strong Lorentz force. This force acts like an retarding force against the flow. So, velocity profiles are diminished along with both directions. The Figures 4 and 5 depict that, for growing values of S, the velocity profile $f'(\eta)$ is declined while $g'(\eta)$ is uplifted. Figures 6 and 7 express that due to growing values of

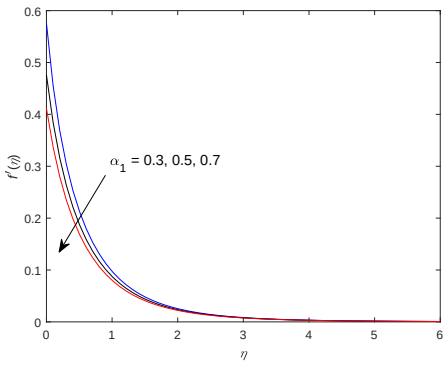

Figure 8. Depiction of $f'(\eta)$ vs α_1

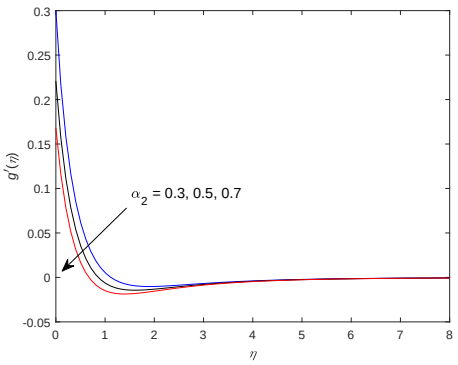

Figure 9. Depiction of $g'(\eta)$ vs α_2

m, $f'(\eta)$ is boosted and a fall in $g'(\eta)$ is noted. For higher values of α_1 and α_2, a diminishing behavior in velocity profiles is seen from Figures 8 and 9. The slip between the fluid and the sheet surface increases as the values of velocity slip parameters increase. As a result, a partial slip velocity is shifted to a flow regime with a tendency to diminish the flow.

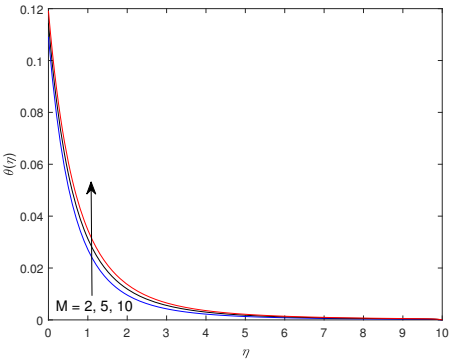

Figure 10. Depiction of $\theta(\eta)$ vs M

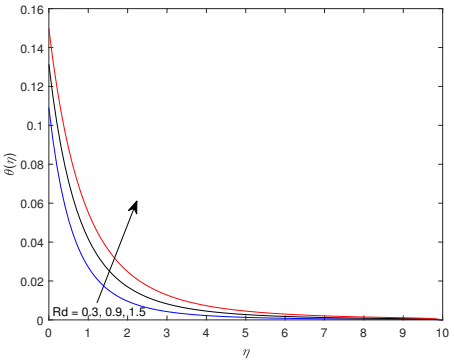

Figure 11. Depiction of $\theta(\eta)$ vs Rd

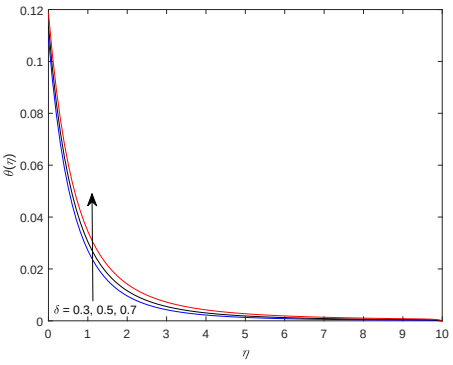

Figure 12. Depiction of $\theta(\eta)$ vs δ

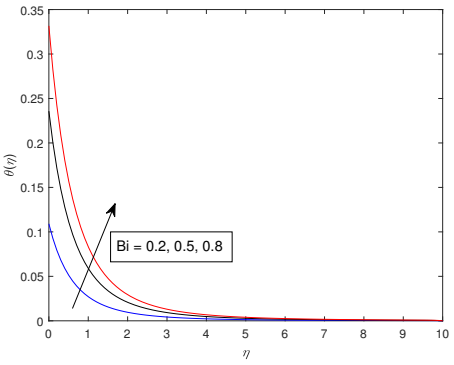

Figure 13. Depiction of $\theta(\eta)$ vs Bi

Figures 10-13 are delineated to examine the behavior of M, Rd, δ and Bi on thermal distribution. Figure 10 shows that the fluid temperature $\theta(\eta)$ enhances on rising M. When magnetic parameter increases, a stronger Lorentz force is generated, and this retards the motion. This force is behind the growth of fluid temperature. Figure 11 elucidates raise in $\theta(\eta)$ on enhanced values of Rd. Improved radiation parameter reduces mean absorption coefficient. As a result,

temperature gets boosted. Figure 12 describes that $\theta(\eta)$ is hiked for δ. From Figure 13, an increase in $\theta(\eta)$ is noticed for enlarged values of Bi. Heat transfer by convection to the fluid flow is observed for higher values of Biot number and consequently, the temperature gets augmented.

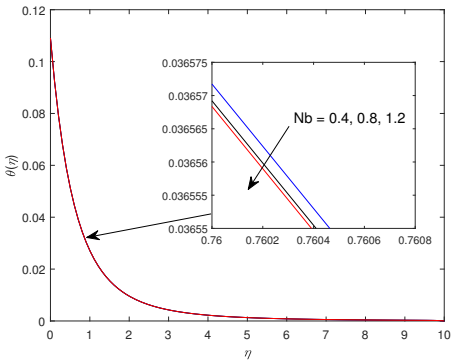

Figure 14. Depiction of $\theta(\eta)$ vs Nb

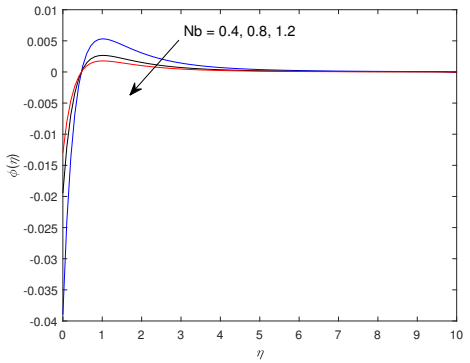

Figure 15. Depiction of $\phi(\eta)$ vs Nb

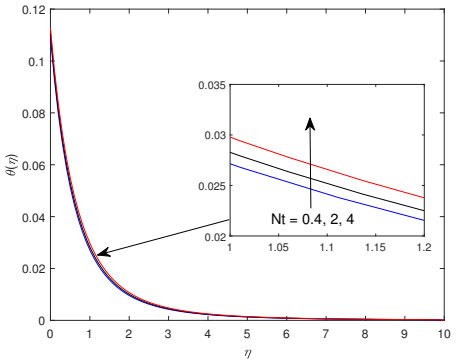

Figure 16. Depiction of $\theta(\eta)$ vs Nt

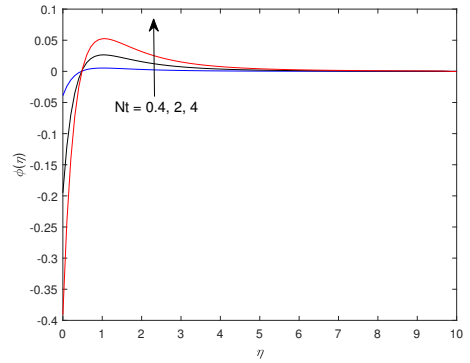

Figure 17. Depiction of $\phi(\eta)$ vs Nt

Figures 14-17 are sketched to analyze the impacts of Nb and Nt on temperature and concentration fields. Figure 14 shows that when Nb increases, $\theta(\eta)$ decreases near the sheet and takes on an inverse nature far away from it. In reality, a larger Nb causes more Brownian diffusion with lesser viscous forces, which raises the fluid temperature. $\phi(\eta)$ is enhanced near the sheet for enhancing Nb values, while the reverse influence is perceived away from the sheet, as shown in Figure 15. According to Figure 16, with upsurging values of Nt, $\theta(\eta)$ is increased. Usually, an increase in Nt causes a stronger thermophoretic force, which enriches the temperature of the fluid. Figure 17 shows that $\phi(\eta)$ decreases towards the sheet, while the opposite trend is seen further away from the sheet with respect to Nt. With the help of Figures 18-19, the influences of Γ_1 and E on concentration profiles are explored. Figure 18 shows that when the value of Γ_1 rises, $\phi(\eta)$ falls. A devastating chemical reaction corresponds to a positive Γ_1. As a result, an improvement in Γ_1 causes a decrease in species concentration. Figure 19 shows that with increasing E values, there is an upward trend in $\phi(\eta)$. Boosted E values aid in the speeding up of chemical reactions. So, $\phi(\eta)$ is increased.

The numerical values of local skin-friction coefficients for various values of the flow parameters S, M, m, α_1 and α_2 are set forth in Table 3. For higher values of M and S, $\sqrt{Re_x}C_{fx}$ is increased whereas reverse trend is detected w.r.t. m and α_1. $\sqrt{Re_y}C_{fy}$ is enhanced for enlarged values of S, M and m while inverse nature is seen w.r.t. α_2. Local Nusselt and Sherwood numbers calculated for flow parameters M, Rd, δ, Bi, Nb, Nt, Γ_1 and E are described in Table 4. Increasing trend of $\frac{Nu_x}{\sqrt{Re_x}}$ is found for Rd, Bi and Nb but opposite nature is for M, δ and Nt. Growing values of Nt and E imply increasing tendency of $\frac{Sh_x}{\sqrt{Re_x}}$ whereas converse behavior is noticed w.r.t. Nb and Γ_1.

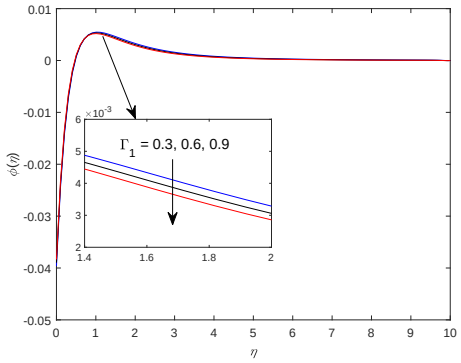

Figure 18. Depiction of $\phi(\eta)$ vs Γ_1

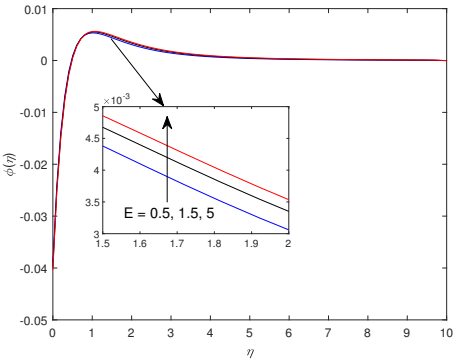

Figure 19. Depiction of $\phi(\eta)$ vs E

Table 3. Numerical values of the local skin friction coefficients

S	M	m	α_1	α_2	$-\sqrt{Re_x}C_{fx}$	$-\sqrt{Re_y}C_{fy}$
1.5	2	0.5	0.3	0.3	1.798259	3.133334
0.7					1.718947	3.124399
1.1					1.761278	3.125611
1.5	5				1.977171	3.613123
	10				2.139699	3.925025
	2	0.7			1.768468	3.209514
		0.9			1.740017	3.246091
		0.5	0.5		1.500465	–
			0.7		1.298884	–
			0.3	0.5	–	2.603057
				0.7	–	2.239737

6 Conclusions

The combined impacts of heat radiation, Hall current, Navier's slip, and activation energy on unsteady MHD Carreau nanofluid flow over a bidirectional stretching sheet are discussed in this study. The following are the notable key points of the current investigation:

- Primary velocity is accelerated for boosting values of m while the reverse trend is seen for M, α_1 and S.
- For improving values of S, secondary velocity is highlighted while decreasing trend is observed for α_2, m and M.
- For boosting values of M, Rd, δ, Bi and Nt temperature profile is escalated.
- Concentration profile is enlarged with rising values of Nt and E whereas the reverse trend is noticed w.r.t. Kr.
- Primary skin-friction coefficient is enhanced w.r.t. S and M whilst opposite tendency is observed for m and α_1. The secondary skin-friction coefficient is hiked for escalating values of M, m and S.
- Local Nusselt number is decelerated for growing values of δ, Nt and M while inverse behavior is found w.r.t. Rd, Nb, and Bi.
- For improving values of Nb and Γ_1, local Sherwood number is reduced while the opposite result is noticed for E and Nt.

Table 4. Numerical values of the local Nusselt and Sherwood numbers

M	Rd	δ	Bi	Nb	Nt	Γ_1	E	$\frac{Nu_x}{\sqrt{Re_x}}$	$-\frac{Sh_x}{\sqrt{Re_x}}$
2	0.3	0.3	0.2	0.4	0.4	0.6	0.5	0.233404	0.178181
5								0.232117	–
10								0.230938	–
2	0.9							0.336333	–
	1.5							0.436746	–
	0.3	0.5						0.232307	–
		0.7						0.231047	–
		0.3	0.5					0.505082	–
			0.8					0.711581	–
			0.2	0.8				0.233405	0.089091
				1.2				0.233406	0.059394
				0.4	2			0.233014	0.889316
					4			0.232514	1.774564
					0.4	0.3		–	0.178183
						0.9		–	0.178179
						0.5	1.5	–	0.178183
							5	–	0.178184

References

[1] S. M. AbdEl-Gaied and M. A. A. Hamad, MHD forced convection laminar boundary layer flow of alumina-water nanofluid over a moving permeable at plate with convective surface boundary condition, *J. Appl. Math.* **2013**, 403210 (2013).

[2] A. Aziz and W. Jamshed, Unsteady MHD slip flow of non Newtonian power-law nanofluid over a moving surface with temperature dependent thermal conductivity, *Discrete Contin. Dyn. Syst. - S* **11(4)**, 617–630 (2018).

[3] A. Bhattacharyya, G. S. Seth and R. Kumar, Modeling of viscoelastic fluid flow past a non-linearly stretching surface with convective heat transfer: OHAM analysis, *Math. Model. Sci. Comput. Appl.* **308**, 297–312 (2020).

[4] A. J. Chamkha, A. M. Aly and M. A. Mansour, Similarity solution for unsteady heat and mass transfer from a stretching surface embedded in a porous medium with suction/injection and chemical reaction effects, *Chem. Eng. Commun.* **197(6)**, 846–858 (2010).

[5] R. Cortell, Flow and heat transfer of an electrically conducting fluid of second grade over a stretching sheet subject to suction and to a transverse magnetic field, *Int. J. Heat Mass Transf.* **49(11–12)**, 1851–1856 (2006).

[6] Y. S. Daniel, Z. A. Aziz, Z. Ismail and F. Salah, Effects of thermal radiation, viscous and Joule heating on electrical MHD nanofluid with double stratification, *Chin. J. Phys.* **55(3)**, 630–651 (2017).

[7] M. Das, S. Nandi, B. Kumbhakar and G. S. Seth, Soret and Dufour effects on MHD nonlinear convective flow of tangent hyperbolic nanofluid over a bidirectional stretching sheet with multiple slips, *J. Nanofluids* **10(2)**, 200–213 (2021).

[8] M. R. Eid and K. L. Mahny, Unsteady MHD heat and mass transfer of a non-Newtonian nanofluid flow of a two-phase model over a permeable stretching wall with heat generation/absorption, *Adv. Powder Technol.* **28(11)**, 3063–3073 (2017).

[9] E. O. Fatunmbi and A. Adeniyan, Nonlinear thermal radiation and entropy generation on steady flow of magneto-micropolar fluid passing a stretchable sheet with variable properties, *Results Eng.* **6**, 100142 (2020).

[10] B. J. Gireesha, M. Umeshaiah, B. C. Prasannakumara, N. S. Shashikumar and M. Archana, Impact of nonlinear thermal radiation on magnetohydrodynamic three dimensional boundary layer flow of Jeffrey nanofluid over a nonlinearly permeable stretching sheet, *Physica A* **549**, 124051 (2020).

[11] S. P. Goqo, S. D. Oloniiju, H. Mondal, P. Sibanda and S. S. Motsa, Entropy generation in MHD radiative viscous nanofluid flow over a porous wedge using the bivariate spectral quasi-linearization method, *Case Stud. Therm. Eng.* **12**, 774–788 (2018).

[12] T. Hayat and M. Qasim, Influence of thermal radiation and Joule heating on MHD flow of a Maxwell fluid in the presence of thermophoresis, *Int. J. Heat Mass Transf.* **53(21–22)**, 4780–4788 (2010).

[13] T. Hayat, M. Imtiaz, A. Alsaedi and M. A. Kutbi, MHD three-dimensional flow of nanofluid with velocity slip and nonlinear thermal radiation, *J. Magn. Magn. Mater.* **396**, 31–37 (2015).

[14] S. M. Ibrahim, P. V. Kumar, G. Lorenzini, E. Lorenzini and F. Mabood, Numerical study of the onset of chemical reaction and heat source on dissipative MHD stagnation point flow of Casson nanofluid over a nonlinear stretching sheet with velocity slip and convective boundary conditions, *J. Eng. Thermophys.* **26**, 256–271 (2017).

[15] M. Irfan, K. Rafiq, M. Khan, M. Waqas and M. S. Anwar, Theoretical analysis of new mass flux theory and Arrhenius activation energy in Carreau nanofluid with magnetic influence, *Int. Commun. Heat Mass Transf.* **120**, 105051 (2021).

[16] M. Irfan, Study of Brownian motion and thermophoretic diffusion on non-linear mixed convection flow of Carreau nanofluid subject to variable properties, *Surf. Interfaces* **23**, 100926 (2021).

[17] N. S. Khan, T. Gul, S. Islam, A. Khan and Z. Shah, Brownian motion and thermophoresis effects on MHD mixed convective thin film second-grade nanofluid flow with Hall effect and heat transfer past a stretching sheet, *J. Nanofluids* **6(5)**, 812–829 (2017).

[18] B. Kumbhakar and P. S. Rao, Dissipative boundary layer flow over a nonlinearly stretching sheet in the presence of magnetic field and thermal radiation, *Proc. Natl. Acad. Sci., India, Sect. A Phys. Sci.* **85**, 117–125 (2015).

[19] I. C. Liu and H. I. Andersson, Heat transfer over a bidirectional stretching sheet with variable thermal conditions, *Int. J. Heat Mass Transf.* **51(15–16)**, 4018–4024 (2008).

[20] M. K. Mishra, G. S. Seth and R. Sharma, Navier's slip effect on mixed convection flow of non-Newtonian nanofluid: Buongiorno's model with passive control approach, *Int. J. Appl. Comput. Math.* **5**, 107 (2019).

[21] M. Mustafa, J. A. Khan, T. Hayat and A. Alsaedi, Buoyancy effects on the MHD nanofluid flow past a vertical surface with chemical reaction and activation energy, *Int. J. Heat Mass Transf.* **108**, 1340–1346 (2017).

[22] S. Nandi and B. Kumbhakar, Unsteady MHD free convective flow past a permeable vertical plate with periodic movement and slippage in the presence of Hall current and rotation, *Therm. Sci. Eng. Prog.* **19**, 100561 (2020).

[23] S. Nandi and B. Kumbhakar, Hall current and thermo-diffusion effects on magnetohydrodynamic convective flow near an oscillatory plate with ramped type thermal and solutal boundary conditions, *Indian J. Phys.* (2021). doi: 10.1007/s12648-020-02001-0

[24] K. V. Prasad, K. Vajravelu and H. Vaidya, Hall effect on MHD flow and heat transfer over a stretching sheet with variable thickness, *Int. J. Comput. Methods Eng. Sci. Mech.* **17(4)**, 288–297 (2016).

[25] M. M. Rashidi, N. V. Ganesh, A. K. A. Hakeem and B. Ganga, Buoyancy effect on MHD flow of nanofluid over a stretching sheet in the presence of thermal radiation, *J. Mol. Liq.* **198**, 234–238 (2014).

[26] G. S. Seth, M. K. Mishra and R. Tripathi, MHD free convective heat transfer in a Walter's liquid-B fluid past a convectively heated stretching sheet with partial wall slip, *J. Braz. Soc. Mech. Sci. Eng.* **40**, 103 (2018).

[27] G. S. Seth, A. Bhattacharyya and M. K. Mishra, Study of partial slip mechanism on free convection flow of viscoelastic fluid past a nonlinearly stretching surface, *Comput. Therm. Sci.: Int. J.* **11(1–2)**, 105–117 (2019).

[28] Z. Shah, E. Bonyah, S. Islam and T. Gul, Impact of thermal radiation on electrical MHD rotating flow of Carbon nanotubes over a stretching sheet, *AIP Adv.* **9(1)**, 015115 (2019).

[29] S. Sharidan, T. Mahmood and I. Pop, Similarity solutions for the unsteady boundary layer flow and heat transfer due to a stretching sheet, *Int. J. Appl. Mech. Eng.* **11(3)**, 647–654 (2006).

[30] R. Sharma, S. M. Hussain, C. S. K. Raju, G. S. Seth and A. J. Chamkha, Study of graphene Maxwell nanofluid flow past a linearly stretched sheet: A numerical and statistical approach, *Chin. J. Phys.* **68**, 671–683 (2020).

[31] S. A. Shehzad, T. Hayat, M. Qasim and S. Asghar, Effects of mass transfer on MHD flow of Casson fluid with chemical reaction and suction, *Braz. J. Chem. Eng.* **30(1)**, 187–195 (2013).

[32] G. C. Shit and R. Haldar, Thermal radiation and hall effect on MHD flow, heat and mass transfer over an inclined permeable stretching sheet, *Therm. Sci.* **15(2)**, 195–204 (2011).

[33] J. K. Singh, G. S. Seth, S. Vishwanath and P. Rohidas, Steady MHD mixed convection flow of a viscoelastic fluid over a magnetized convectively heated vertical surface with Hall current and induced magnetic field effects, *Heat Transf.* **49(8)**, 4370–4393 (2020).

[34] V. K. Sinha, B. Kumar, G. S. Seth and R. Nandkeolyar, Features of Jeffrey fluid flow with Hall current: A spectral simulation, *Pramana* **94**, 64 (2020).

[35] X. Y. Tian, B. W. Li and Z. M. Hu, Convective stagnation point flow of a MHD non-Newtonian nanofluid towards a stretching plate, *Int. J. Heat Mass Transf.* **127(Part A)**, 768–780 (2018).

[36] M. Turkyilmazoglu, The analytical solution of mixed convection heat transfer and fluid flow of a MHD viscoelastic fluid over a permeable stretching surface, *Int. J. Mech. Sci.* **77**, 263–268 (2013).

[37] C. Y. Wang, The three dimensional flow due to a stretching flat surface, *Phys. Fluids* **27**, 1915–1917 (1984).

Author information

Manik Das, Susmay Nandi and Bidyasagar Kumbhakar, Department of Mathematics, National Institute of Technology Meghalaya, Shillong-793003, India.
E-mail: manikdas@nitm.ac.in, nsusmay@nitm.ac.in, bkmath@nitm.ac.in